Biosensors and Bioelectronics 123 (2019) 101–107

Contents lists available at ScienceDirect

Biosensors and Bioelectronics

journal homepage: www.elsevier.com/locate/bios

3D graphene-based foam induced by phytic acid: An effective enzyme-mimic catalyst for electrochemical detection of cell-released superoxide anion

Xuan Cai[a], Huilan Chen[a], Zhenxing Wang[a], Wenqian Sun[a], Libo Shi[a], Hongli Zhao[a,*], Minbo Lan[a,b,**]

[a] Shanghai Key Laboratory of Functional Materials Chemistry, School of Chemistry and Molecular Engineering, East China University of Science and Technology, Shanghai 200237, PR China

[b] State Key Laboratory of Bioreactor Engineering, East China University of Science and Technology, Shanghai 200237, PR China

ARTICLE INFO

Keywords:
Non-enzymatic sensor
Superoxide anion
Living cells
Graphene-based foam

ABSTRACT

Here we present a new method to fabricate enzyme-mimic metal-free catalysts for electrochemical detection of superoxide anion ($O_2^{\bullet -}$) by introducing phosphate groups into graphene-based foam. Through a template-free hydrothermal process, graphene oxide (GO) was treated with different amount of phytic acid (PA) to obtain 3D porous graphene-based foam (PAGF). Characterizations demonstrate that phosphate groups were successfully modified on the surface and inter layer structure of PAGF materials and the defects and disorder degree of PAGF could be controlled by adjusting the addition of PA precursors. Meanwhile, the synthesized PAGF was successfully immobilized on screen printed carbon electrodes (SPCEs) and employed in $O_2^{\bullet -}$ detection. With PA treated on graphene structure, the resulted PAGF/SPCEs exhibit distinct characteristic redox peaks, showing enzyme-mimic catalytic activity toward $O_2^{\bullet -}$ dismutation. Also, the amount of modified phosphate groups has caused a considerable variety on the performance of PAGF-based electrodes. Apart from high sensitivity, wide liner range, low detection limit, good selectivity and long-term stability, our sensors also present satisfying performance in the real-time monitoring of drug-induced $O_2^{\bullet -}$ released from Hela cells. The reliability of the biological measurement was further demonstrated via electron paramagnetic resonance (EPR) to characterize the released $O_2^{\bullet -}$ from stimulated cells by using 2,2,6,6-tetramethylpiperidine-1-oxyl (TEMPOL) to trap the transient $O_2^{\bullet -}$. The above results indicate that our established sensors hold potential application in the real-time detection of $O_2^{\bullet -}$ in biological samples.

1. Introduction

Since the discovery of its crucial role in the pathology of cancers, superoxide anions ($O_2^{\bullet -}$), which is a kind of important Reactive Oxygen Species (ROS), has been considered as a potential biomarker in the diagnosis of cancers and some other significant diseases (Tong et al., 2015; Yamazaki et al., 2011). According to previous research, $O_2^{\bullet -}$ is related with multistage of canceration of normal cells since it can affect the methylation of DNA as well as the signal pathway in living cells, thus impacting the expression of cancer gene (Khandrika et al., 2009; Panayiotidis, 2008; Trachootham et al., 2009). Therefore, the quick analysis and real-time monitoring of $O_2^{\bullet -}$ in biological samples is of great significance. In the past decades, many methods have been developed for the detection of $O_2^{\bullet -}$ such as electron paramagnetic resonance (EPR) (Campbell et al., 1999; Mitchell et al., 2013), fluorescent sensors (Umezawa et al., 1999; Zhang et al., 2018) and electrochemical sensors (Ge et al., 2003; Tian et al., 2004). Among the above methods, electrochemical sensors exhibit short response time, excellent reproducibility and high sensitivity, being regarded as an ideal tool for the dynamic detection of transient $O_2^{\bullet -}$.

Recently, some electrochemical sensors have been developed to catch the signal of cell-released $O_2^{\bullet -}$ (Liu et al., 2015; Sadeghian et al., 2016), however, the quantification of $O_2^{\bullet -}$ in living cells is still difficult due to the low concentration of $O_2^{\bullet -}$ and the existence of many interferences in biological system. Besides, most traditional $O_2^{\bullet -}$ electrochemical sensors are based on enzymes such as superoxide dismutase (SOD) and cytochrome c whose activity could vary along with pH, temperature and other environmental factors (Sadeghian et al., 2016; Zhu et al., 2016, 2015). Therefore, the development of inorganic enzyme-mimic nanomaterials with high catalysis activity is the key to

* Corresponding author.
** Corresponding author at: Shanghai Key Laboratory of Functional Materials Chemistry, School of Chemistry and Molecular Engineering, East China University of Science and Technology, Shanghai 200237, PR China.
E-mail addresses: honglizhao@ecust.edu.cn (H. Zhao), minbolan@ecust.edu.cn (M. Lan).

https://doi.org/10.1016/j.bios.2018.06.043
Received 17 April 2018; Received in revised form 7 June 2018; Accepted 23 June 2018
Available online 25 June 2018
0956-5663/

further improve the performance of $O_2^{\bullet-}$ electrochemical sensors in real sample analysis.

So far, several kinds of enzyme-mimic materials for $O_2^{\bullet-}$ dismutation have been explored mainly includes novel-metal-based materials (Li et al., 2018), transition-metal-based materials (Cai et al., 2018; Shen et al., 2016) and some carbon materials with special structures (Liu et al., 2017a). Among the above nanomaterials, the novel-metal-based catalysts often exhibit obvious response toward several ROS include $O_2^{\bullet-}$ and H_2O_2 at the same time (Huang et al., 2017; Zhang et al., 2016), which could negatively affect the quantitative result of $O_2^{\bullet-}$ sensing. Also, the high price of novel metals has dramatically limited their usage in real samples. As for the transition-metal based compounds, the complicated and time-consuming synthesis process is one of the main limitations of its application (Shen et al., 2016; Wang et al., 2017). Carbon-based materials such as hollow carbon spheres and fullerene are reported to be considerable electrochemical catalysts for $O_2^{\bullet-}$ dismutation due to the electron transfer in the inner structures (Wei and Wang, 2013). Meanwhile, these metal-free materials present high conductivity and good biocompatibility, holding potential use in the electrochemical analysis in biological system. Nevertheless, the mechanism of the enzyme-mimic activity of the above carbon-based catalysts is not clear, thus the research about the design of carbon-based SOD-mimic materials is still very limited. Therefore, the development of novel carbon-based Nanozyme for $O_2^{\bullet-}$ dismutation is significant for enhancing the performance of $O_2^{\bullet-}$ electrochemical sensor and its application in biological samples.

In this work, we present a new method to obtain carbon-based Nanozyme by introducing phosphate groups into graphene-based foam for electrochemical detection of $O_2^{\bullet-}$. After treated with PA, the GO layers were connected to form porous sponge-like products with enhanced conductivity and electrochemical catalysis activity. By adjusting the amount of PA precursor, the defect and disorder degree of resulting products was efficiently controlled. Characterizations demonstrated that the PAGF catalyst with the highest degree of defects and disorders exhibited the highest sensitivity toward $O_2^{\bullet-}$ sensing. Meanwhile, the toxicity of the recommended PAGF catalyst was investigated by MTT assay which demonstrated the excellent biocompatibility of the synthesized material. The fabricated sensor was further applied in the real-time monitoring of cellular $O_2^{\bullet-}$ and the linear correlation between drug-induced $O_2^{\bullet-}$ and the amount of stimulating drug was revealed. Besides, EPR spectra, which is one of the most widely-used methods for $O_2^{\bullet-}$ sensing, was employed to catch Zymosan-induced cellular $O_2^{\bullet-}$, demonstrating the reliability of the electrochemical result. The established sensor in this work present satisfying performance with low detection limit, wide liner range, excellent reproducibility and selectivity, thus has potential usage in clinical diagnosis in the future.

2. Experimental

2.1. Chemicals and apparatus

Graphene powder was commercially purchased from Sinopharm Chemical Reagent Co., Ltd. Concentrated sulfuric acid, phosphoric acid, H_2O_2 (30%) and $KMnO_4$ were obtained from Shanghai Lingfeng Chemical Reagent Co., Ltd. Phytic acid solution (70%), anhydrous dimethyl sulfoxide (DMSO), 18-crown-6 and KO_2 were purchased from Aladdin Industrial Inc. Zymosan, ascorbic acid (AA), dopamine (DA), Acetaminophen (AP) and uric acid (UA) were provided by Sigma-Aldrich. KH_2PO_4, K_2HPO_4, KCl, $NaNO_3$, K_2SO_4, $K_3[Fe(CN)_6]$, $K_4[Fe(CN)_6]$ were provided by Sinopharm Chemical Reagent Co., Ltd. Dulbecco's modified Eagle's medium (DMEM) cell culture medium, penicillin/streptomycin, trypsin, fetal bovine serum (FBS) and thiazole blue tetrazolium bromide (MTT) were bought from Gibco Invitrogen. During all the experiments, ultrapure water used was produced by a Laboratory Water Purification System (18.2 M cm). All the above chemicals were directly used without any further purification.

X-ray diffraction (XRD) patterns of all resulted products were obtained by using a D/MAX2550 diffractometer (Rigaku International Co., Japan). Raman spectra were acquired using an InVia-Reflex Laser Micro-Raman Spectrometer (Renishaw). A scanning electron microscopy (SEM, JSM-6360LV, JEOL) and a JEM-1400 transmission electron microscope (JEOL, Japan) was employed to characterize the morphology of synthesized materials. XPS spectra were obtained using an ESCALAB 250Xispectrophotometer (Thermo Fisher, USA). The fluorescence of 96-well plates in the investigation of cell viability was acquired by using an ELISA instrument (Thermo Scientific Multiskan MK). EPR spectra was acquired from a 100G-18kG/EMX-8/2.7 Electro-Spin Resonance Spectrometer (Bruker Daltonics, USA).

2.2. Synthesis of PAGF catalysts

Graphene oxide (GO) was prepared according to the traditional Hummers' method (Marcano et al., 2010) with some modification. Specifically, 1.5 g graphene powder was dispersed in a mixture of 130 mL concentrated sulfuric acid and 20 mL phosphoric acid in a 500 mL flask. Subsequently, 9 g $KMnO_4$ was slowly added into the flask and the mixture was refluxed at 50 °C for 12 h. After that, the resulting liquid was mixed with 450 mL H_2O in ice water bath and cooled down to room temperature. In order to reduce the remaining $KMnO_4$ in the reaction system, H_2O_2 was added into the above mixture under stirring till the solution turned to light yellow. Then, the suspension was stood overnight to separate the product with clear supernatant. The obtained solid was washed using 3 mol/L HCl solution and ultrapure water until the pH of supernatant turned to around 7. Finally, the GO solid was transferred to a glass-surface vessel and freeze-dried.

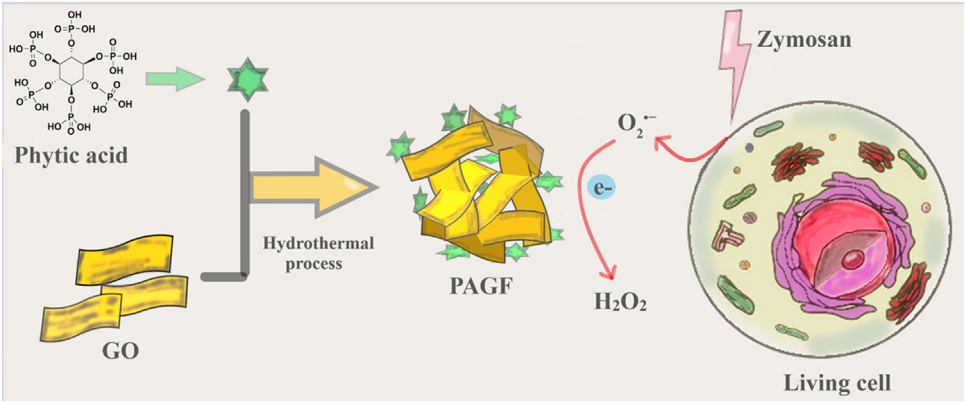

Scheme 1. Illustration of the synthesis of PAGF materials and the detection of cell-released superoxide anions.

The synthesis process of PA treated graphene-based foam (PAGF) was illustrated in the Scheme 1 (Song et al., 2016). In the one-step hydrothermal process, PA was employed to not only reduce graphene oxide sheets and enhance the conductivity, but also introduce phosphate groups which could assemble with the interlayer structures of graphene oxide, forming compact 3D porous foam. Meanwhile, the addition of PA precursor in the reaction system determined the amount of modified phosphate groups in PAGF catalysts. Typically, 0.12 g GO powder was dispersed in 60 mL water by sonicating for 30 min. After that, 2.86 mL PA aqueous solution (70%) was added and the mixture was sonicated for another 40 min. Then, the suspension was transferred into a 100 mL Teflon-lined autoclave and maintained at 180 °C for 12 h. The autoclave was stand overnight and cooled down to room temperature. Finally, the solid was washed with ethanol and ultrapure water for several times and freeze-dried for further use. The resulting product was marked as 1PAGF. By changing the PA volume in the reaction system, the 0.5PAGF (PA 1.43 mL) and 1.5PAGF (PA 4.29 mL) products were obtained using the same method. Also, as comparison, graphene-based foam (GF) without PA treatment was approached through the above process with no PA addition.

2.3. Fabrication of PAGF-based electrochemical sensors

The fabrication of home-made screen-printed carbon electrodes (SPCEs) has been described in our previous work (Zuo et al., 2008). For the preparation of PAGF/SPCEs, the synthesized PAGF catalyst was dispersed in a mixture of ethanol and water to form a 1 mg/mL suspension under ultrasonification. After that, 6 μL of the suspension and 3 μL of Nafion (3%) were drop-casted on the surface of SPCE. The modified electrodes were dried in air and stored in a desiccator for further use. GO/SPCEs and GF/SPCEs were also fabricated through the same process.

2.4. Preparation of $O_2^{\bullet -}$ stock solution

The $O_2^{\bullet -}$ stock solution was prepared by dissolving KO_2 powder into a mixture of DMSO and 18-crown-6 (Liu et al., 2017a; Shen et al., 2016). In this organic system, $O_2^{\bullet -}$ can be stabilized for a relatively long time. The concentration of $O_2^{\bullet -}$ was determined by UV–vis spectra (Hyland and Auclair, 1981; Thandavan et al., 2013).

2.5. Cell culture and MTT assay

Hela cells were cultured in a culture vessel in a 37 °C humid incubator with an atmosphere consisted of 95% air and 5% CO_2. Each vessel contains 5 mL DMEM medium with 10% fetal bovine serum (FBS) and 1% penicillin/streptomycin. The toxicity of materials was investigated by MTT assay using 96-well plates which contained Zymosan (0.5 mg/mL, 0.005 mg/mL, 0.0005 mg/mL and 0.00005 mg/mL) or 1PAGF (1 mg/mL, 0.1 mg/mL, 0.01 mg/mL and 0.001 mg/mL). The control groups were cultured in DMEM medium without Zymosan or 1PAGF. The above 96-well plates were put in the incubator for 24 h. After that, MTT was added into each well and the resulting plates were cultured for another 4 h. Finally, all the cell culture was emptied and 150 μL DMSO was added to each well to detect the fluorescence value by using an ELISA instrument. The cell viability was the mean of three results calculated by the following formula: fluorescence of experimental group / fluorescence of control group × 100%.

2.6. Inflammatory stimulate

After being cultured to exponential phase, the cells were collected through centrifugation (1000 rpm, 5 min) and dispersed in 5 mL PBS for electrochemical sensing. The cell number was counted using a microscopy and was calculated to be 5×10^6. During the electrochemical determination of cell-released $O_2^{\bullet -}$, different amount of Zymosan (5 mg/L) was added into the cell suspension to stimulate the produce of $O_2^{\bullet -}$ from Hela cells. And the concentration of drug-induced $O_2^{\bullet -}$ was determined by the current response of our established sensor. During the EPR assay, 100 μM TEMPOL and 0.5 mg/mL Zymosan A was added into DMEM medium with Hela cells. After cultured for 0.5 h, the EPR spectra of the cell culture medium were obtained by using an Electro-Spin Resonance Spectrometer. The measurement was carried out with microwave frequency of 9.187 GHz and microwave power of 2.016 mW. The sweep time is 41.943 s with a time constant of 163.840 s. As comparison, a same amount of Hela cells were cultured in cell culture contained 100 μM TEMPOL without stimulating drug for 0.5 h, and the resulting cell medium was used in the EPR assay. Also, the EPR spectra of cell medium contained 100 μM TEMPOL without cells was obtained under the same condition.

3. Results and discussions

3.1. Characterizations

In the synthesis of PAGF materials, the multiple phosphate groups of PA located in the edge of hexatomic ring could stack graphene oxide layers with less spatial hindrance, thus “stitching” graphene sheets into 3D networks. Meanwhile, during the hydrothermal process, graphene oxide was reduced by forming stacked structures and the conductivity of resulting materials was enhanced. The images of synthesized materials were displayed in Fig. 1**A**. And the morphology of our products was further visualized by using TEM and SEM characterizations. As shown in Fig. 1**B**, the prepared GO sheets were ultrathin monolayers with folding on the surface. After hydrothermal process, GO can be reduced and thus aggregate as presented in Fig. 1**C**. However, when PA was added into the hydrothermal system, GO layers were not only aggregated but also further stacked to form 3D networks, and the corresponding morphology of 1PAGF was revealed in Fig. 1**D**, presenting thicker structures and network patterns. Also, the similar morphologies of 0.5PAGF and 1.5PAGF were listed in the TEM images of Fig. S1. To further visualize the structure of PAGF materials, SEM characterization was carried out and the results were shown in Figs. 1**E** and 1**F**, corresponding to the SEM images of graphene-based materials before and after treated with PA. As a result, it is obvious that 1PAGF exhibit porous structures which were absent in GO precursor, indicating that the resulting 1PAGF material was sponge-like foam. Meanwhile, the similar structure of 0.5PAGF and 1.5PAGF were demonstrated in Fig. S2.

Besides, the XRD patterns of GO, GF and 1PAGF were shown in Fig. S3. As a result, the lines of GF and 1PAGF presented a wide peak at around 24.9°, corresponding to the (002) plane of aggregated structures of graphene. Also, the peak intensity of 1PAGF was stronger than that of GF, indicating higher stacking degree of graphene layers in 1PAGF after induced by PA, which was also demonstrated in the above TEM patterns. To further reveal the degree of disorders and defects in prepared PAGF catalysts with different PA addition, the Raman spectra of 0.5PAGF, 1PAGF and 1.5PAGF were presented in Fig. 2**A**. The D band is located at around 1340 cm^{-1} and the G band 1580 cm^{-1}. The ratios of intensities of the above two bands (I_D/I_G) were calculated to be 1.42, 1.51 and 1.46, corresponding to the result of 0.5PAGF, 1PAGF and 1.5PAGF, respectively. Concluded from the above data, 1PAGF exhibit the highest degree of disorder and defect, thus containing more active sites for electron transfer (Liu et al., 2017a). The values of I_D/I_G were increased by 6.3% when PA addition enlarged from1.43 mL to 2.86 mL. However, the I_D/I_G value declined when the amount of PA during the reaction was further increased to 4.29 mL. This is because that too much PA covered on the surface of GO sheets can reduce the active sites for inter-layer stacking and the formation of 3D networks (Song et al., 2016). The elemental states of 1PAGF were further investigated by using XPS characterization. Observed from the wide survey spectrum of Fig. 2**B**, the synthesized 1PAGF material mainly contains three kinds of

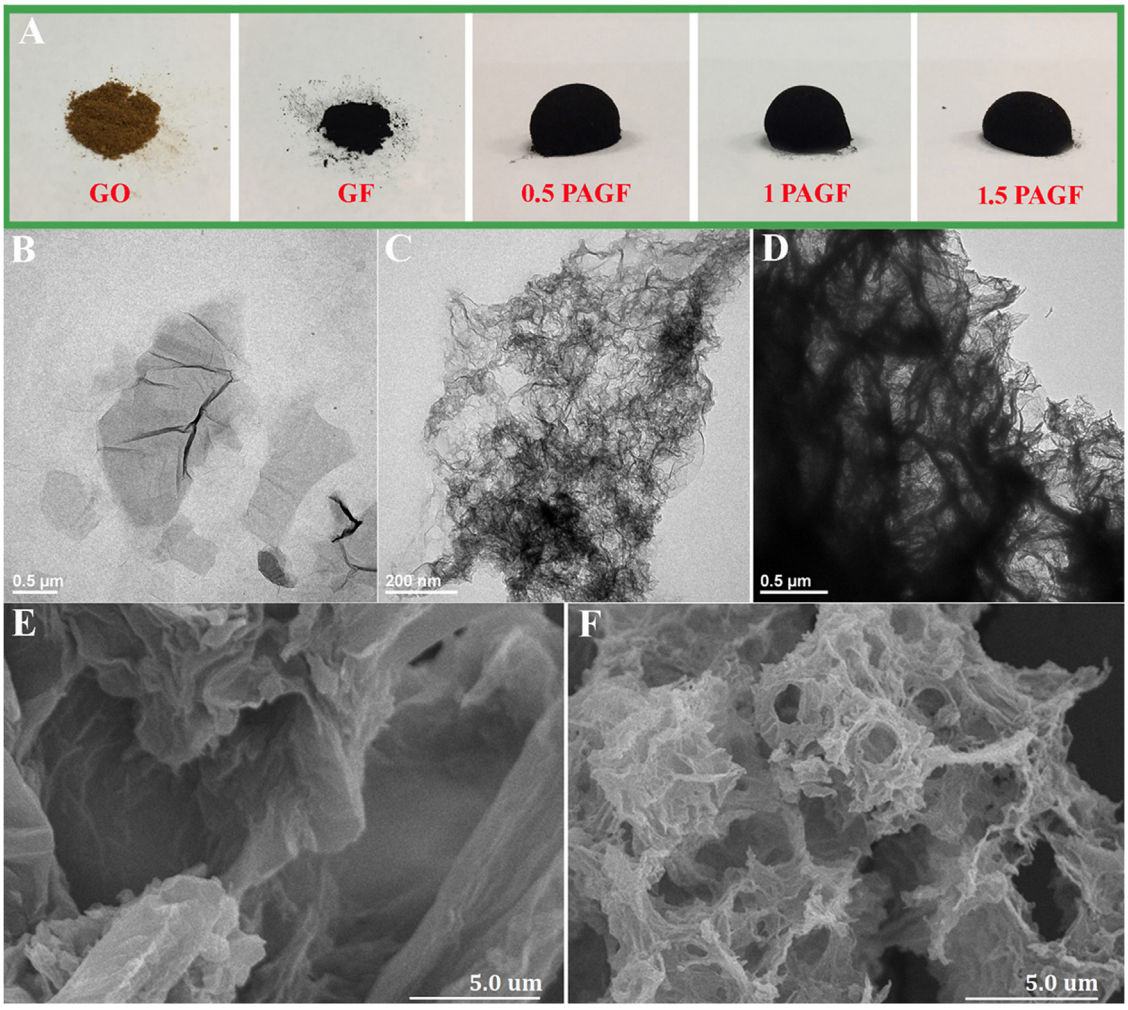

Fig. 1. (A) Images of synthesized materials. TEM characterization of **(B)** GO, **(C)** GF and **(D)** 1PAGF. SEM images of **(E)** GO and **(F)** 1PAGF.

elements which are P (134.5 eV, 191 eV), C (284.8 eV) and O (532.7 eV). The high resolution XPS spectra of C1s, O1s and P2p were presented in Fig. S4, indicating that the phosphorous groups were successfully connected into the graphene structure. The above XPS results are in consistent with the relevant references (Araujo et al., 2016; Song et al., 2016).

3.2. Electrochemical behaviour of PAGF-based sensors

The above synthesized materials were drop-casted on the home-made screen printed carbon electrodes (SPCE) and directly employed in the superoxide sensing. Firstly, the electrochemical characteristics of modified electrodes were investigated by using cyclic voltammetry (CV) at a potential range of − 0.8 to 0.6 V. As shown in Fig. 3**A**, GO presents no obvious redox peaks, however, after the hydrothermal process, the

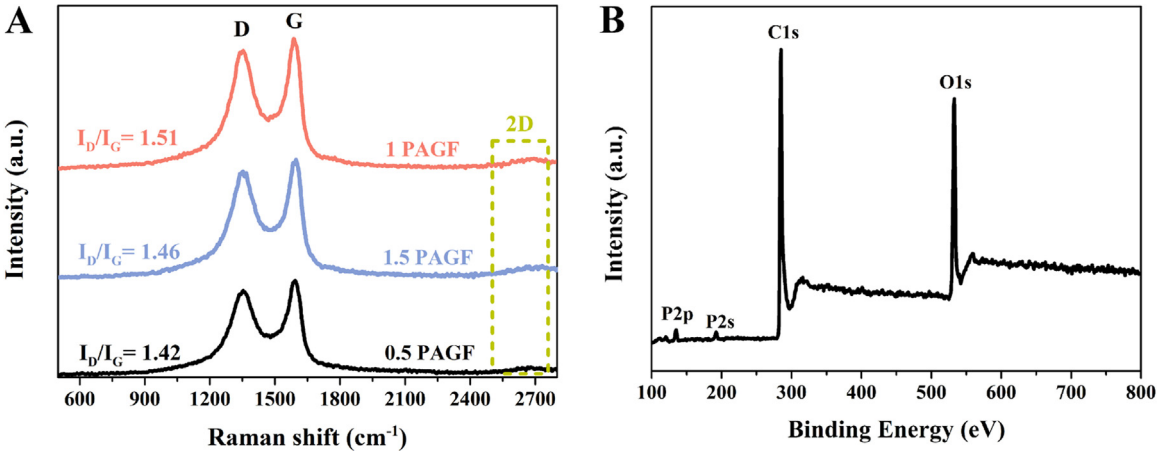

Fig. 2. (A) Raman spectra of PAGF materials prepared through hydrothermal process with different additions of PA. **(B)** XPS survey spectrum of 1PAGF.

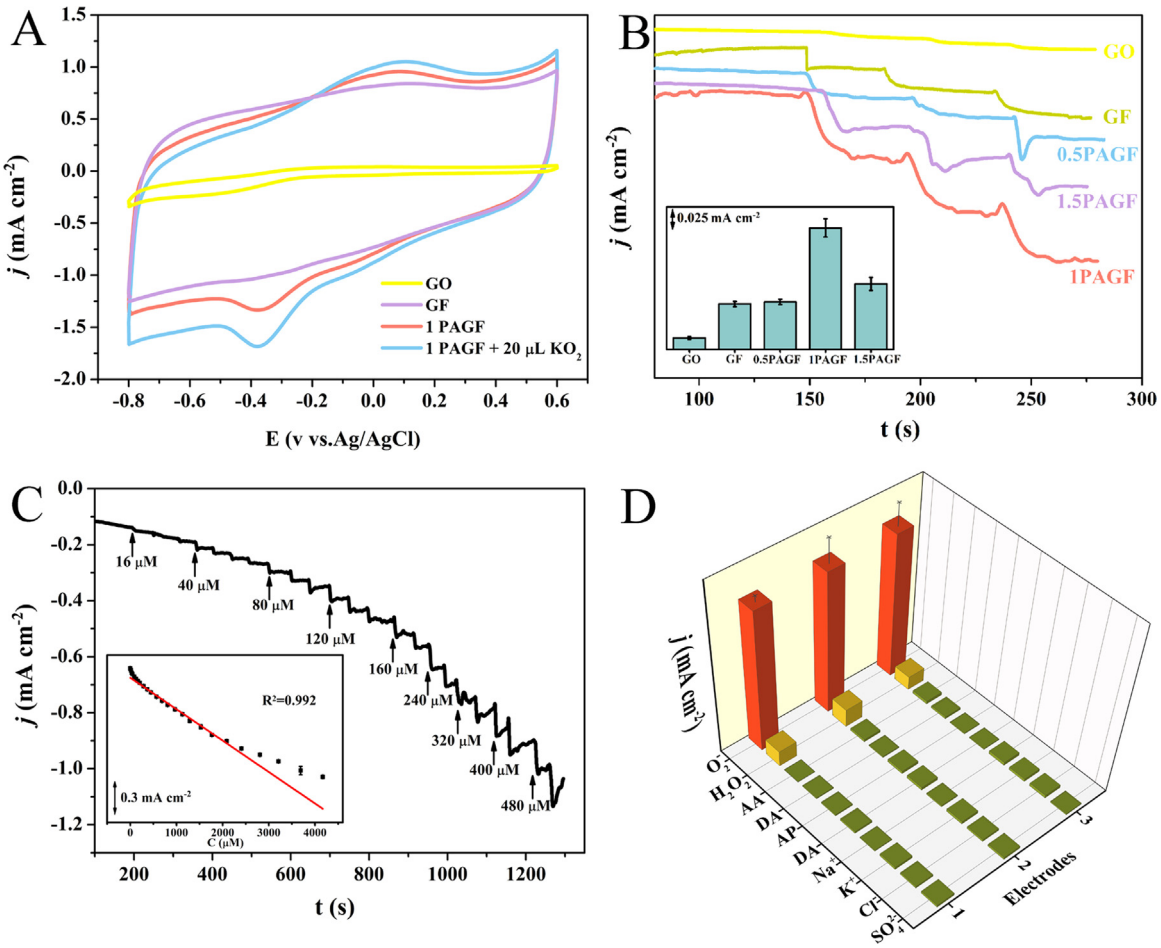

Fig. 3. (A) Cyclic voltammetry curves of fabricated electrodes in 0.1 M PBS with and without the addition of 0.16 mM $O_2^{\bullet -}$ in 5 mL 0.1 M PBS at a scan rate of 50 mV/s in the potential range of − 0.8 to 0.6 V. **(B)** The amperometric responses of different modified electrodes at the addition of 0.08 mM $O_2^{\bullet -}$ in 5 mL 0.1 M PBS at each step. Applied potential: − 0.4 V. **(C)** The amperometric responses and fitted line of 1PAGF/SPCEs toward different addition of $O_2^{\bullet -}$ in 5 mL 0.1 M PBS under an applied potential of − 0.4 V. **(D)** The current responses of three 1PAGF/SPCEs toward 0.08 mM $O_2^{\bullet -}$ and H_2O_2 as well as 0.5 mM AA, DA, AP, UA, Na^+, K^+, SO_4^{2-} and Cl^-. Applied potential: − 0.4 V.

resulting GF exhibits a pair of wide redox peaks at the potential ranges of − 0.5 to − 0.3 V and − 0.1 to 0.1 V. Interestingly, both redox currents were obviously increased after the GO was treated with PA, and the redox peaks of 1PAGF became sharper. The above characteristic peaks correspond to the electron transfer in the carbon structures. After the introduction of phosphorous groups and the hydrothermal reduction of GO, the defects and disorder degree of the products were increased. Therefore, compared with GO and GF, the PAGF materials contains more active sites for electron transfer, thus exhibiting larger redox current and higher electrochemical catalysis activity (Liu et al., 2017a). At the addition of 0.16 mM $O_2^{\bullet -}$, both redox currents of 1PAGF increased as shown in Fig. 3**A**, demonstrating that 1PAGF can catalyse both reduction and oxidation of $O_2^{\bullet -}$. The dismutation of $O_2^{\bullet -}$ can be illustrated as follows:

$$O_2^{\bullet -} + e^- + H_2O \rightarrow H_2O_2 \quad (1)$$

$$O_2^{\bullet -} - e^- + H^+ \rightarrow O_2 + H_2O \quad (2)$$

Besides, the CV curves of 0.5PAGF and 1.5PAGF in 0.1 M PBS were also presented in Fig. S5, indicating their similar catalysis ability toward $O_2^{\bullet -}$ dismutation.

Before the quantitative detection of target analyst, the applied potential, which could greatly impact the current responses of electrochemical sensors, was optimized by using chronoamperometry. As shown in Fig. S6, the current responses of 1PAGF/SPCEs were recorded at the addition of 0.08 mM $O_2^{\bullet -}$ at each step in a potential range of − 0.6 to − 0.2 V. As a result, our modified electrodes exhibit highest sensitivity at the applied potential of − 0.4 V. Thus, the following electrochemical detection of $O_2^{\bullet -}$ were carried out at the optimized potential of − 0.4 V. To further evaluate the electrochemical catalysis activity of different synthesized materials, the amperometric responses of GO/SPCEs, GF/SPCEs, 0.5PAGF/SPCEs, 1PAGF/SPCEs and 1.5PAGF/SPCEs toward 0.08 mM $O_2^{\bullet -}$ were recorded as shown in Fig. 3**B**. Obviously, the 1PAGF/SPCEs present the biggest response at the addition of $O_2^{\bullet -}$. This is because that 1PAGF materials have more active sites for the adhesion and electrochemical reaction of target analyst, thus exhibiting higher sensitivity toward $O_2^{\bullet -}$ determination. The above results demonstrate that the introduction of phosphorous groups in the graphene-based foam could enlarge its degree of defects and disorders, thus increase the active sites for electron transfer and improve the sensitivity toward target analyst.

3.3. Performance evaluation of 1PAGF/SPCEs

The performance of the recommended 1PAGF/SPCEs was further systematically evaluated. As shown in Fig. 3**C**, the real time i-t curve was recorded at the different addition of $O_2^{\bullet -}$ into 0.1 M PBS at a potential of − 0.4 V. Previous researches have revealed that the normal concentration of $O_2^{\bullet -}$ in biological system is between 10 and 100 nM and can rise to 0.1 mM when the related diseases occur (Liu et al., 2017b; Xue et al., 2000), therefore the liner range of superoxide sensors

should cover the entire range of $O_2^{\bullet -}$ concentrations. The inset image in Fig. 3**C** shows that our sensors exhibit a wide liner range of 0–4.168 mM with a square of correlation coefficient of 0.992, indicating that the recommended 1PAGF/SPCEs have potential usage in biological samples. Compared with some previous researches in Table S1, our electrodes in this work present higher sensitivity (300.3 μA cm^{-2} mM^{-1}), lower detection limit (0.141 μM, S/N = 3) and wider liner range.

In biological samples, there are usually many kinds of potential interferences which could affect the current responses, thus the selectivity of established sensors should be evaluated before real sample analysis. Among the various biological interferences, H_2O_2, which is another kind of ROS, is always considered as one of the main species which could affect the $O_2^{\bullet -}$ detection since H_2O_2 can be generated during the reduction of $O_2^{\bullet -}$ and the metabolism of many other chemicals in biological system. As shown in Fig. 3**D**, 0.08 mM $O_2^{\bullet -}$ and H_2O_2 were added into 0.1 M PBS to investigate the current response of 1PAGF/SPCEs toward the two kinds of ROS. The results show that the response toward 0.08 mM H_2O_2 is only 9.8% of that caused by 0.08 mM $O_2^{\bullet -}$, which is acceptable during the detection of $O_2^{\bullet -}$ (Shen et al., 2016). Besides, some other potential interferences, such as 0.5 mM AA, DA, AP, UA, Na^+, K^+, SO_4^{2-} and Cl^- were added into the same system to record the corresponding signals. As shown in Fig. 3**D**, our sensors didn`t exhibit any obvious current responses toward the above species, demonstrating that the 1PAGF/SPCEs have excellent selectivity in $O_2^{\bullet -}$ determination.

Besides, the reproducibility of the modified electrodes was also investigated by using three 1PAGF/SPCEs prepared at the same time to detect 0.08 mM $O_2^{\bullet -}$. The results in Fig. 3**D** indicate that the recommended sensors hold satisfying reproducibility with an RSD of 0.83%. Last but not the least, the long-term stability of the 1PAGF/SPCEs was studied by collecting the signal variation of modified electrodes toward 0.08 mM $O_2^{\bullet -}$ in a period of one month and the electrodes were stored at room temperature when not used. As shown in Fig. S7, the current responses of our sensors didn`t have obvious decline after 30 days, indicating an outstanding long-term stability.

3.4. Dynamic detection of cell-released $O_2^{\bullet -}$

Real-time and dynamic detection of cell-release $O_2^{\bullet -}$ can provide important data for the pathological study and diagnosis of some significant diseases such as cancers (Tong et al., 2015). Therefore, in this section the established sensors were used to capture the transient signal of drug-stimulated cellular $O_2^{\bullet -}$. First of all, the DMEM cell culture, which may contains some potential interference, was employed in the real sample analysis. Typically, $O_2^{\bullet -}$ of different concentrations were added into a mixture of 1 mL DMEM culture and 4 mL 0.1 M PBS to record the current responses. As comparison, the same detection process was carried out by using 5 mL PBS without cell medium. As shown in Table. S2, The recovery was calculated to be 98.33%, 98.52% and 105.12% at the addition of 0.08 mM, 0.16 mM and 0.24 mM $O_2^{\bullet -}$, respectively, indicating that our sensor can be used in the real samples. Meanwhile, the toxicity of 1PAGF catalysts in Hela cells was investigated. As shown in Fig. S8A, the cell viabilities of Hela cells cultured in DMEM cell medium contained 1PAGF (0.001–1 mg/mL) were more than 100%, demonstrating that the carbon-based 1PAGF catalysts have excellent biocompatibility. Also, the toxicity of Zymosan used in the stimulation of Hela cells was studied using the same method. The result in Fig. S8B shows all the cell viabilities are over 80%, indicating that the concentrations of Zymosan used in this work, which is in the range of 00005–0.5 mg/mL is appropriate for Hela cells.

During the determination of cellular $O_2^{\bullet -}$, Zymosan A was employed to stimulate living cells to produce ROS include $O_2^{\bullet -}$ and the current variation was detected using the established sensors. As shown in Fig. 4, when different volumes of Zymosan A were added into the system, the current density instantly increased due to the reduction of cell-released $O_2^{\bullet -}$ and remained steady for a few seconds. As

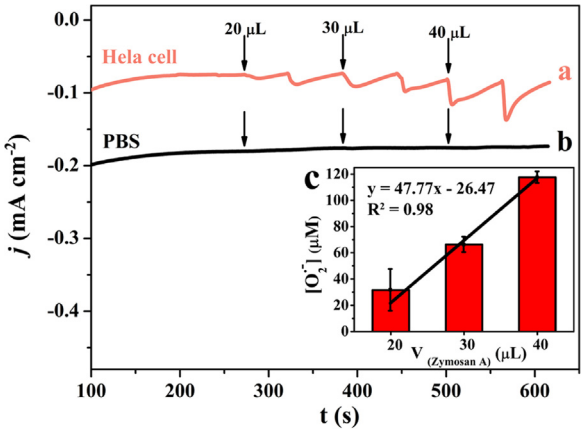

Fig. 4. The current responses of 1PAGF/SPCEs at the stimulating of 20 μL, 30 μL and 40 μL 10 mg/mL Zymosan A in 5 mL 0.1 M PBS with **(a)** and without **(b)** Hela cells. The inset image **(c)**: the liner fitted result of cell-released $O_2^{\bullet -}$ versus the volume of stimulating drug.

comparison, the same volumes of Zymosan A were added into 0.1 M PBS without Hela cells under the same condition. As a result, no obvious current changes occurred as shown in the line b of Fig. 4, indicating that the current responses of line a were attributed to cell-released $O_2^{\bullet -}$ rather than the stimulating drug. Also, the current densities collected from a same amount of Hela cells dispersed in PBS and DMEM, respectively, were also studied as shown in Fig. S9. When no stimulating drug was added, the current densities of the above two samples were almost the same and remained unchanged during the whole process, indicating that the current response in Fig. 4 were caused by drug-induced $O_2^{\bullet -}$ and the existence of DMEM would not obviously impact the detecting of cellular $O_2^{\bullet -}$. Furthermore, according to sensitivity of our sensors and the current density of line a in Fig. 4, the concentrations of drug-induced $O_2^{\bullet -}$ were calculated to be 31.5 μM, 66.2 μM and 117.6 μM at the stimulation of 20 μL, 30 μL and 40 μL Zymosan A (20 mg/mL), respectively. In the whole system, the cell number was about 5×10^6, therefore the average amount of $O_2^{\bullet -}$ released from every single cell could be estimated to be 6.3 pM, 13.24 pM and 23.52 pM at different addition of Zymosan A in this study. Furthermore, the liner dependency between the drug-induced $O_2^{\bullet -}$ (μM) and the amount of stimulating drug (μL) was also revealed as shown in the inset image c of Fig. 4. The liner equation was fitted to be y (μM) = 47.77 × (μL) − 26.47 (R^2 = 0.98), indicating that the produce of drug-induced $O_2^{\bullet -}$ is a concentration-dependent process (Cai et al., 2018).

Besides, EPR spectroscopy, which is one of the most widely-used methods for ROS determination, was employed to further check the reliability of electrochemical detection of cell-released $O_2^{\bullet -}$. TEMPOL is widely-used as the spin-trap of $O_2^{\bullet -}$ since it can combine with transient $O_2^{\bullet -}$ to form stable compound for EPR assay (Yamasaki et al., 2013). Therefore, in this section TEMPOL was used to trap cell-released $O_2^{\bullet -}$ and the EPR spectra was presented in Fig. S10. As a result, the peak intensity of TEMPOL slightly decreased after the living cells were added into the system. This declined signal was probably caused by the naturally produced $O_2^{\bullet -}$ from living cells. When Zymosan A was added into the system, the peak intensity of TEMPOL was obviously cut down as shown in the red line of Fig. S10 due to the combination between TEMPOL and $O_2^{\bullet -}$. This result further demonstrated the existence of drug-induced $O_2^{\bullet -}$ released by Hela cells under the stimulation of Zymosan, confirming the reliability of our established sensor when used in the determination of stimulated $O_2^{\bullet -}$.

4. Conclusions

In this work, a novel Nanozyme for $O_2^{\bullet -}$ dismutation was developed

by introducing phosphate groups into graphene-based foam. The electrochemical catalysis activity of the prepared PAGF materials is mainly determined by its degree of defects and disorders which can be efficiently controlled by adjusting the amount of PA precursor during the synthesis process. This investigation provides a new way to design carbon-based metal-free catalysts as the substitution of natural SOD. Meanwhile, the established 1PAGF/SPCEs sensors exhibit satisfying performance of high sensitivity, good selectivity and low detection limit toward the quantitation of $O_2^{\bullet -}$. Furthermore, the fabricated sensors were successfully employed in the determination of cell-released $O_2^{\bullet -}$ and present excellent performance in the dynamic monitoring of cellular $O_2^{\bullet -}$. On the other hand, the main limitation of this work lies on the semi-quantification result of cell-released $O_2^{\bullet -}$ which should be further improved by advancing the sensitivity and detection limit of electrochemical sensor to realize the accurate quantification of $O_2^{\bullet -}$ in cellular environment in the future.

Acknowledgements

This research was financially supported by the Science and Technology Commission of Shanghai Municipality (STCSM, No. 16520710800) and the Fundamental Research Funds for the Central Universities (No. 222201817022).

Appendix A. Supplementary material

Supplementary data associated with this article can be found in the online version at http://dx.doi.org/10.1016/j.bios.2018.06.043.

References

Araujo, J.R., Silva, A.M., Gouvea, C.P., Lopes, E.S., Santos, R.A.A., Terrazos, L.A., Capaz, R.B., Achete, C.A., Maciel, I.O., 2016. Phosphorous bonding in single wall carbon nanotubes studied by X-ray photoelectron spectroscopy and DFT calculations. Carbon 99, 1–7.

Cai, X., Shi, L., Sun, W., Zhao, H., Li, H., He, H., Lan, M., 2018. A facile way to fabricate manganese phosphate self-assembled carbon networks as efficient electrochemical catalysts for real-time monitoring of superoxide anions released from HepG2 cells. Biosens. Bioelectron. 102, 171–178.

Campbell, K.A., Yikilmaz, E., Grant, C.V., Gregor, W., Miller, A.F., Britt, R.D., 1999. Parallel polarization EPR characterization of the Mn(III) center of oxidized manganese superoxide dismutase. J. Am. Chem. Soc. 121 (19), 4714–4715.

Ge, B., Scheller, F.W., Lisdat, F., 2003. Electrochemistry of immobilized CuZnSOD and FeSOD and their interaction with superoxide radicals. Biosens. Bioelectron. 18 (2–3), 295–302.

Huang, B., Wang, Y., Lu, Z., Du, H., Ye, J., 2017. One pot synthesis of palladium-cobalt nanoparticles over carbon nanotubes as a sensitive non-enzymatic sensor for glucose and hydrogen peroxide detection. Sens. Actuators B: Chem. 252, 1016–1025.

Hyland, K., Auclair, C., 1981. The formation of superoxide radical anions by a reaction between O_2, OH^- and dimethyl sulfoxide. Biochem. Biophys. Res. Commun. 102 (1), 531–537.

Khandrika, L., Kumar, B., Koul, S., Maroni, P., Koul, H.K., 2009. Oxidative stress in prostate cancer. Cancer Lett. 282 (2), 125–136.

Li, H., Zhao, H., He, H., Shi, L., Cai, X., Lan, M., 2018. Pt-Pd bimetallic nanocoral modified carbon fiber microelectrode as a sensitive hydrogen peroxide sensor for cellular detection. Sens. Actuators B: Chem. 260, 174–182.

Liu, L., Zhao, H., Shi, L., Lan, M., Zhang, H., Yu, C., 2017a. Enzyme- and metal-free electrochemical sensor for highly sensitive superoxide anion detection based on nitrogen doped hollow mesoporous carbon spheres. Electrochim. Acta 227, 69–76.

Liu, T., Niu, X., Shi, L., Zhu, X., Zhao, H., Lana, M., 2015. Electrocatalytic analysis of superoxide anion radical using nitrogen-doped graphene supported Prussian Blue as a biomimetic superoxide dismutase. Electrochim. Acta 176, 1280–1287.

Liu, Y., Liu, X., Liu, Y., Liu, G., Ding, L., Lu, X., 2017b. Construction of a highly sensitive non-enzymatic sensor for superoxide anion radical detection from living cells. Biosens. Bioelectron. 90, 39–45.

Marcano, D.C., Kosynkin, D.V., Berlin, J.M., Sinitskii, A., Sun, Z., Slesarev, A., Alemany, L.B., Lu, W., Tour, J.M., 2010. Improved synthesis of graphene oxide. Acs Nano 4 (8), 4806–4814.

Mitchell, D.G., Rosen, G.M., Tseitlin, M., Symmes, B., Eaton, S.S., Eaton, G.R., 2013. Use of rapid-scan EPR to improve detection sensitivity for spin-trapped radicals. Biophys. J. 105 (2), 338–342.

Panayiotidis, M., 2008. Reactive oxygen species (ROS) in multistage carcinogenesis. Cancer Lett. 266 (1), 3–5.

Sadeghian, R.B., Ostrovidov, S., Han, J., Salehi, S., Bahraminejad, B., Bae, H., Chen, M., Khademhosseini, A., 2016. Online monitoring of superoxide anions released from skeletal muscle cells using an electrochemical biosensor based on thick-film nanoporous gold. ACS Sens. 1, 921–928.

Shen, X., Wang, Q., Liu, Y., Xue, W., Ma, L., Feng, S., Wan, M., Wang, F., Mao, C., 2016. Manganese phosphate self-assembled nanoparticle surface and its application for superoxide anion detection. Sci. Rep. 6, 28989.

Song, X., Chen, Y., Rong, M., Xie, Z., Zhao, T., Wang, Y., Chen, X., Wolfbeis, O.S., 2016. A phytic acid induced super-amphiphilic multifunctional 3D graphene-based foam. Angew. Chem. Int. Ed. Engl. 55 (12), 3936–3941.

Thandavan, K., Gandhi, S., Sethuraman, S., Rayappan, J.B.B., Krishnan, U.M., 2013. A novel nano-interfaced superoxide biosensor. Sens. Actuators B-Chem. 176, 884–892.

Tian, Y., Mao, L.Q., Okajima, T., Ohsaka, T., 2004. Electrochemistry and electrocatalytic activities of superoxide dismutases at gold electrodes modified with a self-assembled monolayer. Anal. Chem. 76 (14), 4162–4168.

Tong, L., Chuang, C.C., Wu, S., Zuo, L., 2015. Reactive oxygen species in redox cancer therapy. Cancer Lett. 367 (1), 18–25.

Trachootham, D., Alexandre, J., Huang, P., 2009. Targeting cancer cells by ROS-mediated mechanisms: a radical therapeutic approach? Nat. Rev. Drug Discov. 8 (7), 579–591.

Umezawa, N., Tanaka, K., Urano, Y., Kikuchi, K., Higuchi, T., Nagano, T., 1999. Novel fluorescent probes for singlet oxygen. Angew. Chem. Int. Ed. Engl. 38 (19), 2899–2901.

Wang, M.Q., Ye, C., Bao, S.J., Xu, M.W., Zhang, Y., Wang, L., Ma, X.Q., Guo, J., Li, C.M., 2017. Nanostructured cobalt phosphates as excellent biomimetic enzymes to sensitively detect superoxide anions released from living cells. Biosens. Bioelectron. 87, 998–1004.

Wei, H., Wang, E., 2013. Nanomaterials with enzyme-like characteristics (nanozymes): next-generation artificial enzymes. Chem. Soc. Rev. 42 (14), 6060–6093.

Xue, J.A., Xian, Y.Z., Ying, X.Y., Chen, J.S., Wang, L., Jin, L.T., 2000. Fabrication of an ultramicrosensor for measurement of extracellular myocardial superoxide. Anal. Chim. Acta 405 (1–2), 77–85.

Yamasaki, T., Matsuoka, Y., Mito, F., Yamato, M., Yamada, K.-i., 2013. Redox potential of nitroxides is an index to evaluate superoxide dismutase mimic activity. Asian J. Org. Chem. 2 (5), 388–391.

Yamazaki, T., Kawai, C., Yamauchi, A., Kuribayashi, F., 2011. A highly sensitive chemiluminescence assay for superoxide detection and chronic granulomatous disease diagnosis. Trop. Med. Health 39 (2), 41–45.

Zhang, H., Bo, X., Guo, L., 2016. Electrochemical preparation of Pt nanoparticles supported on porous graphene with ionic liquids: electrocatalyst for both methanol oxidation and H_2O_2 reduction. Electrochim. Acta 201, 117–124.

Zhang, Z., Fan, J., Zhao, Y., Kang, Y., Du, J., Peng, X., 2018. A mitochondria-accessing ratiometric fluorescent probe for imaging endogenous superoxide anion in live cells and Daphnia magna. ACS Sens.

Zhu, X., Liu, T., Zhao, H., Shi, L., Li, X., Lan, M., 2016. Ultrasensitive detection of superoxide anion released from living cells using a porous Pt-Pd decorated enzymatic sensor. Biosens. Bioelectron. 79, 449–456.

Zhu, X., Niu, X., Zhao, H., Tang, J., Lan, M., 2015. Immobilization of superoxide dismutase on Pt-Pd/MWCNTs hybrid modified electrode surface for superoxide anion detection. Biosens. Bioelectron. 67, 79–85.

Zuo, S., Teng, Y., Yuan, H., Lan, M., 2008. Direct electrochemistry of glucose oxidase on screen-printed electrodes through one-step enzyme immobilization process with silica sol–gel/polyvinyl alcohol hybrid film. Sens. Actuators B: Chem. 133 (2), 555–560.